Alexandria Engineering Journal (2022) 61, 4977–4994

HOSTED BY

Alexandria University

Alexandria Engineering Journal

www.elsevier.com/locate/aej
www.sciencedirect.com

Compact UWB Vivaldi Tapered Slot Antenna

Sahar Saleh [a], Widad Ismail [a,*], Intan Sorfina Zainal Abidin [a], Moh'd Haizal Jamaluddin [b], Mohammed H. Bataineh [c], Asem S. Alzoubi [c]

[a] School of Electrical and Electronic Engineering, Universiti Sains Malaysia, Penang 14300, Malaysia
[b] Wireless Communication Centre, Universiti Teknologi Malaysia, Johor 81310, Malaysia
[c] Hijjwai Faculty for Engineering Technology, Yarmouk University, Irbid 21163, Jordan

Received 13 March 2021; revised 5 September 2021; accepted 21 September 2021
Available online 2 October 2021

KEYWORDS

Ultra-Wideband (UWB);
Vivaldi Tapered Slot Antenna (VTSA);
Microstrip to Slot (M/S) transitions;
CST

Abstract In this paper compact Ultra Wideband (UWB) Vivaldi Tapered Slot Antenna (VTSA) is designed simply by changing its Microstrip to Slot line (M/S) transition. To explain the effect of transition's shapes on the size and the performance of the UWB VTSA, four models (A–D) with detailed parametric studies are analyzed, designed, and fabricated. As compared to Model A, in Model D the size (42.9 mm × 29.28 mm = 1256.112 mm^2) is reduced by 19.25%, and the bandwidth (10.34 GHz) is enhanced by 24.56%, in addition, it provides 6.51 dBi maximum realized gain, and stable end-fire radiation pattern. The validity of the proposed antennas is proven by hardware measurement results.

1. Introduction

UWB (3.1–10.6 GHz) technology has special characteristics such as simpler transceiver structures, low radiated power, large channel capacity, resistance to jamming, ability to work with a small signal-to-noise ratio (SNR), low probability of detection, and inception and immune to multipath effect [1]. To work in UWB, the antenna must have large Bandwidth (BW) and stable radiation pattern such as a Tapered Slot antenna (TSA). Among different broadband antennas, Vivaldi TSA (VTSA) with exponential taper profile is preferred due to its simple planner structure, low profile, lightweight, low fabrication cost, and easy integration with circuits. In addition to its ability to radiate a short pulse with a constant phase center and provide stable symmetrical end-fire radiation pattern and narrow beamwidth [2]. High gain antennas are required to overcome the path loss problem (signal attenuation) and as compared to other broadband antennas such as Crossed Monopole, Conical, Bowtie, and TEM, VTSA provides the highest gain [3]. According to these special characteristics, VTSA is used in UWB See Through Wall (STW) [4], Ground Penetrating Radar (GPR) [5–8] and near field imaging [9], microwave and millimeter-wave imaging [2,10–14], and vehicular communication [15] applications. Many miniaturization techniques have been made on VTSA such as adding corrugations only [16], corrugations and grating elements [12,17], and eliminating the need for baluns or any transition feeding as in Antipodal Vivaldi Antenna (AVA) [10], however, AVA suffers

* Corresponding author.
E-mail addresses: sahar_saleh@student.usm.my (S. Saleh), eewidad@usm.my (W. Ismail), intan.sorfina@usm.my (I.S.Z. Abidin), haizal@utm.my (M.H. Jamaluddin), mohbat@yu.edu.jo (M.H. Bataineh), Asem@yu.edu.jo (A.S. Alzoubi).

Peer review under responsibility of Faculty of Engineering, Alexandria University.

https://doi.org/10.1016/j.aej.2021.09.055

from high cross-polarization which can be mitigated by adding corrugations to the aperture edge [18–24]. In [5], authors used corrugations and the resistive film to enhance the matching and directivity, respectively of the designed wideband (1–5 GHz) VTSA. Short pin and chip resistor were loaded to the microstrip stub and slot line, respectively of compact VTSA in [26] to broaden its BW (1–20 GHz) and increase its gain (7.8 dB). In [27], [28] and [29], different shapes of corrugations are added to enhance BW, matching, radiation characteristics and gain (or directivity) for UWB VTASs, square cosine profile TSA and binomial transformer TSA, respectively. A compact VTSA with a novel small size wideband collinear M/S transition, a metallic reflector and a fork shaped metallic carrier was proposed in [30] for Wireless Personal Area Network (WPAN). In [31], for wideband application, courragations of invert-L slots edge (ILSE) shape was added to the proposed VTSA to extend the matching BW from 2.25 GHz to more than 12 GHz. However, in [16] corrugations were added to design a compact (0.07–0.3 GHz) VTSA with 40% size reduction for water detection application. In [32], authors designed UWB VTSA with low cross-polarization below −30 dB using low permittivity substrate material. In [33] stepped connection between slotline and tapered patch was used to improve the BW (3–15.1 GHz) of the proposed compact UWB TSA. Printed lenses were added in [34] to the aperture of the wideband (1–3 GHz) VTSA to enhance its gain and reduce the Side Lobe Levels (SLLs), respectively. Authors in [35], designed a WLAN (4.9–5.935 GHz) VTSA with high directivity and resistivity against car polarization distortion suitable for vehicular wireless communication. The directivity of this antenna was improved by adding corrugations and directors to the metal layer and aperture of the tapered radiating slot, respectively. Resistive loading and patches are added in addition to corrugations (comb slots) to design a compact wideband (0.4–4 GHz) VTSA in [36]. For more high gain, authors in [37] used Substrate Integrated Waveguide (SIW) feeding technique. Genentic algortitm was used for optimization process to enhance the gain (12.27 dBi) of UWB VTSA in [38]. Inhomogeneous with Anisotropic Zero-Index Metamaterials (AI-ZIM) and Epsilon-Near-Zero Artificial Metamaterials (IA-ENZ-AM) were inserted in the aperture of UWB VTSA to enhance its gain (BW and matching) in [39] and [40], respectively. Dissymmetrical matching structure is used in [41] to reduce the cross polarization effect, reduce the circuit area and enhance BW of the proposed VTSA. For mm Wave applications and UWB ground and space application, high gain 60 GHz and UWB (1–14 GHz) VTSA with efficient performance was designed in [42] and [43] by loading dielectric substrate material in front of the antenna taper slot and adding DGSs and dielectric lens, respectively. Ultrathin Microwave-Absorbing Materials (MAMs) were added in [44] to the UWB VTSA's side edges to enhance its radiation pattern. Dielectric Sheets were used to cover the the Conventional Vivaldi Antenna (DSCVA) in [45] to enhance the gain without increasing the antenna size, by coupling the space wave to be radiated in the end-fire direction. Furthermore, for extra high gain, the designed antenna was elongated with a trapezoid-shaped profile (SP-DSCVA). For further antenna impedance matching, a stripline patch (reactive) was added to the feed line of the wideband (6–8 GHz) VTSA [46].

In this work, compactness is achieved simply by changing the feeding transition shapes and performing detailed parametric studies to get the optimum design parameters avoiding any difficulties of the previous techniques. In addition, the proposed compact antenna provides moderate gain, good S_{11}, and enhanced BW.

The main feeding technique for most TSAs is Microstrip to Slot line (M/S) transition in different shapes. Table 1, illustrates some chosen UWB TSAs in the literature which are not using any gain or bandwidth (BW) enhancement techniques to understand the effect of the M/S transition shapes on the antenna performance. Although the best matching is obtained using (Radial/Rectangular) M/S transition [50], (Circular/Circular) M/S transition [51] in addition to its good matching, it provides higher peak gain, enhanced BW, and smaller area. In this work, to prove how (Circular/Circular) M/S transition helps in reducing the UWB VTSA size and enhancing its performance, four different M/S transition shapes as shown in Table 2 and Fig. 1 are used to feed it. Among the four shapes, (Circular/Circular) M/S transition provides the smallest VTSA size with the best performance. This article contains three other sections: Section 2 talks about VTSA, Section 3 is the main section that explains the design of each model with detailed parametric studies, and finally, Section 4 demonstrates the results and discussions. Rogers RO4003C with $\varepsilon_r = 3.55$, height (h) = 0.813 mm and copper thickness = 0.035 mm is selected for this work. The simulations in this work are carried out using Computer Simulation Technology (CST) software which is based on the Finite Integration Technique (FIT).

2. Vivaldi Tapered Slot Antenna (VTSA)

Vivaldi antenna is a traveling wave TSA and was first proposed by Gibson in 1979 for broadband application [52]. It is called a traveling-wave antenna because when the wave is coupled from the microstrip line to slot line, its energy is tightly bound to the opening width (W_{min}) and as the wave leaked from the transition moving toward the aperture width (W_{max}), its energy becomes weaker and the wave is radiated to the free space from the tapered antenna slot [52]. As it is shown from the configuration of VTSA in Fig. 1(a), a quarter-wave slot with length L_{qw} is connected to the exponentially tapered slot which is defined by [53]

$$y(x) = \pm A e^{r*x} \tag{1}$$

where A is half the minimum width of the tapered slot W_{min} and r is the taper or the magnification factor rate. x is the position along the taper slot length (L_T). Both r and L_T have a significant effect on the antenna performance especially its BW and gain.

According to [53] for best performance,

$$L_T > \lambda_g, \tag{2}$$

where $\lambda_g = \frac{c}{f_c\sqrt{\varepsilon_{eff}}}$ is the guided wavelength at $f_c = 6.85$ GHz (center operating frequency), and

$$W_{\max 1} < W_{\max} < W_{\max 2} \tag{3}$$

where

$$W_{max1} \approx \lambda_0 \quad (\text{at } f_c = 6.85 \text{ GHz}) \tag{3.1}$$

$$W_{\max 2} \approx \lambda_{\min}/2 \tag{3.2}$$

Table 1 UWB TSAs with different M/S transition shapes.

Ref.	Substrate h(mm)/εr	S_{11}(dB) at Frequency Band (GHz)	Gain(dBi)	Tech. to enhance Gain or BW	M/S transition	Size mm × mm
[47]	1.6/4.4	< −10 at 0.9–9.6	3.15–6.3	———	Radial/Circular	300 × 193
[48]	1.6/4.4	< −10 at 3–8	2–5	———	Radial/Diamond	62.6 × 32.5
[49]	0.787/2.2	< −9.38 at2.5–10.6	4–8.4	———	Radial/Radial	82 × 60
[50]	1.27/6.15	< −13.3 at 2.1–9.2	max = 6.12	———	Radial/Rectangular	97 × 124
[51]	**0.5/2.65**	**< −11.3 at 2.4–11.5**	**6.9–14.5**	———	**Circular/Circular**	**150 × 80**

Table 2 The four different M/S transitions used to feed the proposed UWB VTSA.

Model	Model A	Model B	Model C	Model D
M/S transition	Rectangular/Rectangular	Taper/Taper	Trapezoidal/rectangular	Circular/Circular

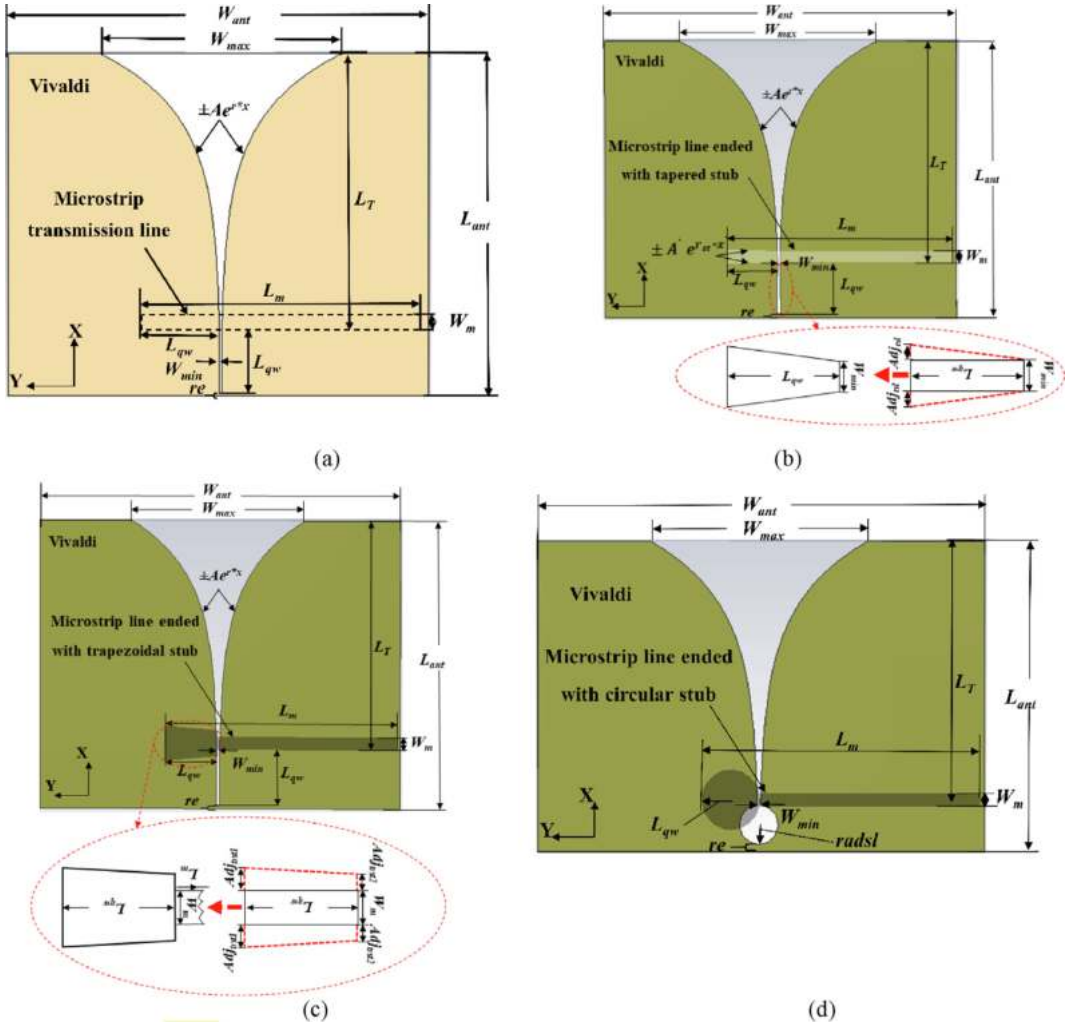

Fig. 1 Layouts of the proposed UWB VTSA models (a) A, (b) B, (c) C, and (d) D.

where, λ_{min} is at Fl = 3.1 GHz.

From the antenna configuration in Fig. 1(a), L_m is the length of the microstrip feed line which is equal to half the antenna width (W_{ant}) added to L_{qw}. The width of the microstrip feed line is represented by W_m and finally, re is the remaining distance of the non-slotted copper in the X-axis.

The excitation in this antenna is happened due to the electromagnetic coupling between the microstrip and slot lines in the transition. The equivalent circuit of this transition is shown in Fig. 2(b). The capacitive effect of the open-ended microstrip line (stub) and inductive effect of the short-ended slot line are represented by the series X_m and shunt X_s reactances, respectively. Z_{0m} and Z_{0s} are the characteristics impedances of microstrip and slot lines, respectively. The coupling between these two lines is represented by the n:1 transformer [54]. For a simpler uniform M/S (Model A: rectangular/rectangular) transition shown in Fig. 1(a), the length of both microstrip and slot lines L_{qw} is selected to be $\lambda g/4$ (at f_c = 6.85 GHz) that provides good matching from the microstrip line feeding to the aperture slot. Due to the importance of this transition, it should be designed properly to get good impedance matching between the low impedance of the microstrip line and the high impedance of the slot line in addition to obtain enhanced BW and gain [55]. Since the antenna BW and matching are limited due to its frequency-dependent parameters in the transition X_s and X_m [53,54], the enhancement can be obtained by controlling the transition parameters and also changing the shape of the transition [55]. The effect of changing the shape of M/S transition is highly affecting the antenna performance and in this work, the focus is on how to exploit this effect in reducing the size of the antenna while maintaining a good in-band matching performance.

3. Design of compact UWB VTSA

At the UWB frequency band (3.1–10.6 GHz) with f_c = 6.85 GHz and using Rogers RO4003C as substrate material, the antenna with four M/S transitions shapes (Model A to D) is designed and simulated using CST. According to (2) and (1), L_T and W_{max} are selected to be 27 mm (> 26.2 mm at f_c = 6.58 GHz) and 24.24 mm (23.24 mm < W_{max} < 25.68 mm), respectively. In each model, parametric studies are performed using CST. The calculated and optimized parameters of all models are illustrated in Table 3 at the end of Section 3.4.

3.1. UWB VTSA with (Rectangular/Rectangular) M/S Transition: (Model A)

The layout of this antenna is the same as the one shown in Fig. 1(a). Fig. 3 shows the parametric studies in terms of S_{11} and gain for Model A on r, L_T, L_{qw}, W_{min}, dis and W_m, respectively, where $dis = W_{ant} - L_{qw}$. The optimized parameters are in a red solid line with a red dashed box. According to (1), r will affect W_{max} which in turn affects the antenna gain [52]. However, larger values will affect X_m and X_s over the entire UWB frequency band and it should be chosen carefully to guarantee the matching [53]. So, there should be a compromise between its value and the M/S transition parameters such as W_{min}, and L_{qw}. Fig. 3(a) shows that at r smaller or greater than 0.159, S_{11} > −10 dB and as r increases, the gain increases. Although the gain is higher at r = 0.164, r = 0.159 is selected for its better matching. The gain in the traveling-wave antenna is directly proportional to L_T which is related to the overall antenna length ($L_{ant} = L_T + L_{qw} + re$) [52] and according to (1) as L_T increases, W_{max} will increase by increasing x. As W_{max} increases, the amount of radiated energy from the aperture increases (gain increases). As shown in Fig. 3(b) when L_T decreases or increases there is a slight shift in the band toward the higher (Fh) and lower (Fl) frequencies, respectively. At L_T less (26.2 mm) or greater (29.4 mm) than L_T = 28.6 mm, the BW is limited due to the effect of frequency-dependent parameters in the M/S transition, X_s and X_m. Fig. 3(b) also shows that although both L_T = 28.6 mm and L_T = 29.4 mm give higher peak gain, L_T = 28.6 mm is selected due to it's better matching (S_{11} < −10.48 dB).

Proper design and selection of the VTSA M/S transition parameters such as L_{qw} and W_{min} should be taken into account to enhance its BW. As L_{qw} decreases or increases, there is a shift in the band toward Fh and Fl, respectively as depicted in Fig. 3(c). Also, the BW and the gain are enhanced as L_{qw} decreases as at L_{qw} = 6.47 mm (BW = 7.7 GHz, and maximum gain = 7.59 dBi), however, the obtained S_{11}(< −10.31 dB) is not that good as compared to the other values. Although at the calculated L_{qw} = 6.57 mm (S_{11} < −10.5 dB, the obtained BW = 7.59 GHz and

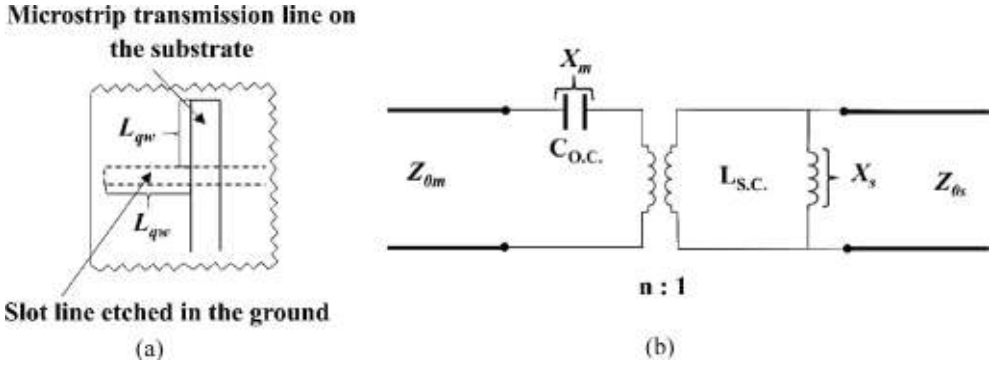

Fig. 2 (a) M/S transition of VTSA (b) Its equivalent circuit [55].

Table 3 Calculated and optimized parameters of the four models.

Parameters	Cal.	Opt.			
Models		A	B	C	D
r	–	0.159	0.159	0.161	0.17
W_{max} (mm)	24.45	24.48	24.49	21.04	21.03
L_T (mm)	27	28.6	27.8	26.4	25
L_{qw} (mm)	6.57	6.52	6.5	6.51	5.7
W_{min} (mm)	–	0.27	0.3	0.3	0.3
radst (mm)	3.285	–	–	–	2.85
radsl (mm)	3.285	–	–	–	1.89
r_{st} (mm)	–	–	0.2	–	–
Adj_{tsl} (mm)	–	–	0.12	–	–
Adj_{trst1} (mm)	–	–	–	2.5	–
Adj_{trst2} (mm)	–	–	–	1.5	–
Adj_{trsl1} (mm)	–	–	–	0	–
Adj_{trsl2} (mm)	–	–	–	0	–
dis(mm)	–	37.4	37.4	36.85	37.2
W_m (mm)	1.819	1.4	1.38	1.55	1.2
re (mm)	–	0.2	0.6	0.35	0.5
L_{ant} (mm)	–	35.42	34.9	33.26	29.28
Want (mm)	–	43.92	43.9	43.36	42.9

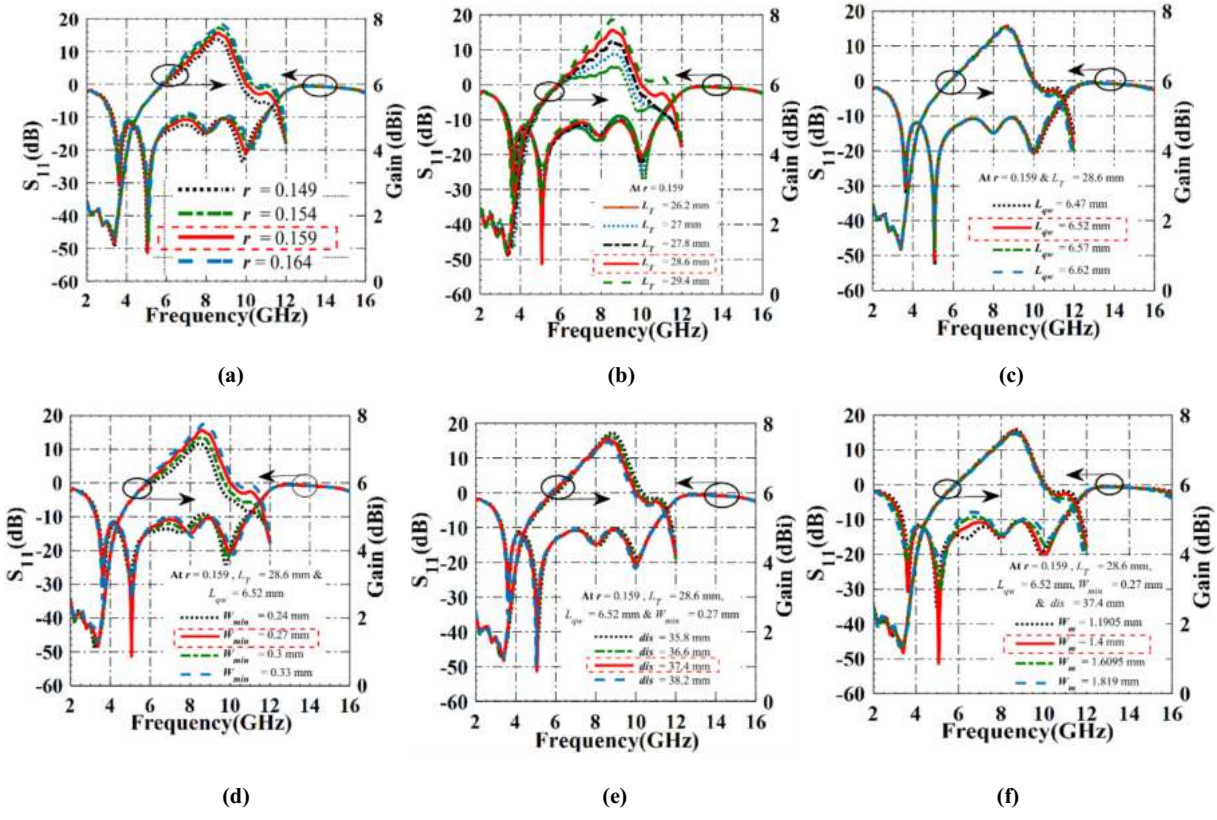

Fig. 3 Parametric study of the proposed UWB VTSA (Model A) in terms of S_{11} and gain on (a) r, (b) L_T, (c) L_{qw}, (d) W_{min}, (e) *dis*, and (f) W_m.

maximum gain = 7.54 dBi) the matching is 0.19% better, L_{qw} = 6.52 mm (S11 < −10.48 dB, the obtained BW = 7.65 GHz and maximum gain = 7.56 dBi) is selected due its 0.78% and 0.26% better BW and gain, respectively. Since W_{min} is related to the slot line impedance in the M/S transition, it will affect the BW. To enhance the BW, *Fl* in the UWB frequency band should be reduced to provide good in-band impedance matching [37]. As depicted in Fig. 3(d),

gain increases, and the BW shifts toward Fl when W_{min} increases with a mismatch at higher values such as at W_{min} = 0.3 mm and 0.33 mm. On the other hand, matching is enhanced as W_{min} decreases and W_{min} = 0.27 mm is selected with optimum BW, gain, and matching.

At the optimized value L_{qw} = 6.52 mm, *dis* is changed to analyze the effect of W_{ant} on the antenna performance. Fig. 3(e), illustrates that there is no big effect on the BW as *dis* changes. Since at *dis* = 37.4 mm and 38.2 mm the BW is almost the same (7.65 GHz), *dis* = 37.4 mm is selected for more compactness. Although the gain is better at small values of *dis* = 36.6 mm and *dis* = 35.8 mm, the matching and BW at *dis* = 37.4 mm are better. As shown in Fig. 3(f), W_m which is related to the width of 50 SMA connector mainly affects the antenna matching. However, it has a small effect on both the BW and the gain and the best-obtained S_{11} is at W_m = 1.4 mm which is better than the calculated one (1.819 mm) due to the effect of the matching between the microstrip and slot line impedances in the transition [53].

The radial stub is a matching transmission line used widely to provide wide BW due to its low impedance level [56] and to analyze its effect, the $\lambda/4$ rectangular stub is replaced by a radial one with a radius equal to L_{qw} as shown in Fig. 4(a). Fig. 4(b) shows that when the angle of the stub (*ang*) decreases or increases, the BW shifts toward *Fl* or *Fh*, respectively. Rad. St. in Fig. 4(b) and (c) is an abbreviation for radial stub. The best matching is obtained at *ang* = 30°, however, the BW is not enhanced (S_{11} < −11.2 dB, BW = 3.04–10.15 = 7.11 G Hz). Although at *ang* = 90°, the BW is wider (S_{11} < 10.3 dB, BW = 3.82–11.42 = 7.61 GHz) than at *ang* = 30°, *Fl* is far away from the required one in the UWB frequency band (3.1–10.6 GHz). To overcome this shift in the obtained BW, a further parametric study is performed on L_{qw} as depicted in Fig. 4(c). At smaller L_{qw}, the BW is enhanced but *Fl* is still around 3.9 GHz and also S_{11} became worse. However, as L_{qw} increases, the BW decreases, and *Fl* shifts toward 4 GHz. So, using radial stub in this model has no advantage in terms of BW or matching. The circuit area for this model is 43.92 × 35.32 mm^2 = 1551.6464 mm^2.

3.2. UWB VTSA with (Tapered/Tapered) M/S Transition: (Model B)

The layout of this model is shown in Fig. 1(b). The exponential tapered profile for the microstrip line in the M/S transition is defined by

$$y'(x') = \pm A' e^{r_{st} * x'} \quad (4)$$

where A' is half the minimum width of the tapered stub in the transition (W_{min1}) and this should be equal to W_m, however, smaller values are better for the antenna matching as will be explained later. r_{st} is the stub taper rate and x' is the position along the tapered stub length (L_{qw}). Due to the small area of the slot in the transition, the exponential taper profile is not used and instead of that a certain value Ad_{jtsl} (adjusting the tapering slot) is added to one side of the $\lambda/4$ rectangular slot to get the tapered shape as shown in the inset of Fig. 1(b). Detailed parametric studies in terms of S_{11} and gain are shown in Fig. 5. The result of the study on *r* is the same as that obtained for Model A where the best performance is achieved at *r* = 0.159 as depicted in Fig. 5(a). The change in L_T causes a slight shift in the band as shown in Fig. 5(b) with best S_{11} at L_T = 27.8 mm (S_{11} < −10.667 dB and maximum realized gain = of 7.39 dBi), although of the higher gain at L_T = 28.6 mm (S_{11} < −10.215 dB and maximum realized gain = of 7.7 dBi). As it is shown in Fig. 5(c), the BW and gain are enhanced as L_{qw} decreases as at L_{qw} = 6.43 mm (S_{11} < −10.731 dB, BW = 3.25–10.96 = 7.71 GHz and maximum gain = 7.4 dBi) in which they are 1.43% and 0.14%, respectively better than that at L_{qw} = 6.5 mm (S_{11} < −10.66 dB, BW = (3.23–10.83) = 7.6 GHz and maximum gain = 7.39 dBi). However, L_{qw} = 6.5 mm is selected due to its smaller *Fl*. Also the matching, BW and gain at L_{qw} = 6.5 mm are 0.66%, 1.45% and 0.27% and 1.41%, 2.1% and 0.54% better than at the calculated one at L_{qw} = 6.57 mm (S_{11} < −10.59 dB, BW = 3.21–10.7) = 7.4 9 GHz and maximum gain = 7.37 dBi) and L_{qw} = 6.64 mm (S_{11} < −10.51 dB, BW = 3.139–10.58 = 7.441 GHz and maximum gain = 7.35 dBi), respectively and this due to the tapered stub and slot shape which is not the case in Model A. As shown in Fig. 5(d) at W_{min} less than or greater than 0.3 mm, there is a mismatch through the UWB frequency band and the best S_{11} is obtained at W_{min} = 0.3 mm (S_{11} < −10. 667 dB and maximum realized gain = of 7.39 dBi) although of the higher gain at W_{min} = 0.5 mm (7.77 dBi). Fig. 5(e), illustrates that the effect of changing r_{st} is small on the BW and the best matching within UWB is obtained at r_{st} = 0.2. Larger values of W_{min1} are not good as compared to that obtained at W_{min1} = 0.2 mm as shown in Fig. 5(f), in addition, changing W_{min1} doesn't mainly change the gain.

As illustrated in Fig. 5(g), at the smallest and largest values of Adj_{tsl} (0.04 mm and 0.16 mm), the BW is shifted toward *Fh* and *Fl*, respectively and the matching is not good as compared

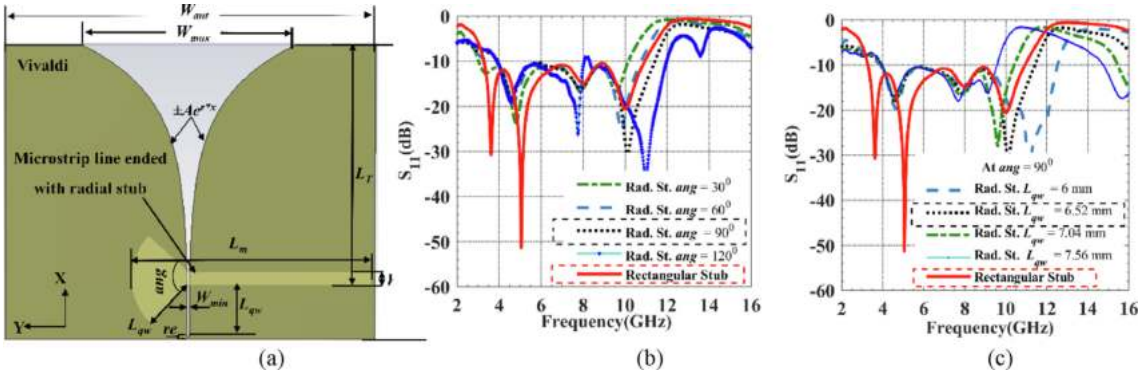

Fig. 4 Layout (a) and S_{11} parametric study on (b) *ang* and (c) L_{qw} of the UWB VTSA with (Radial/Rectangular) M/S transition.

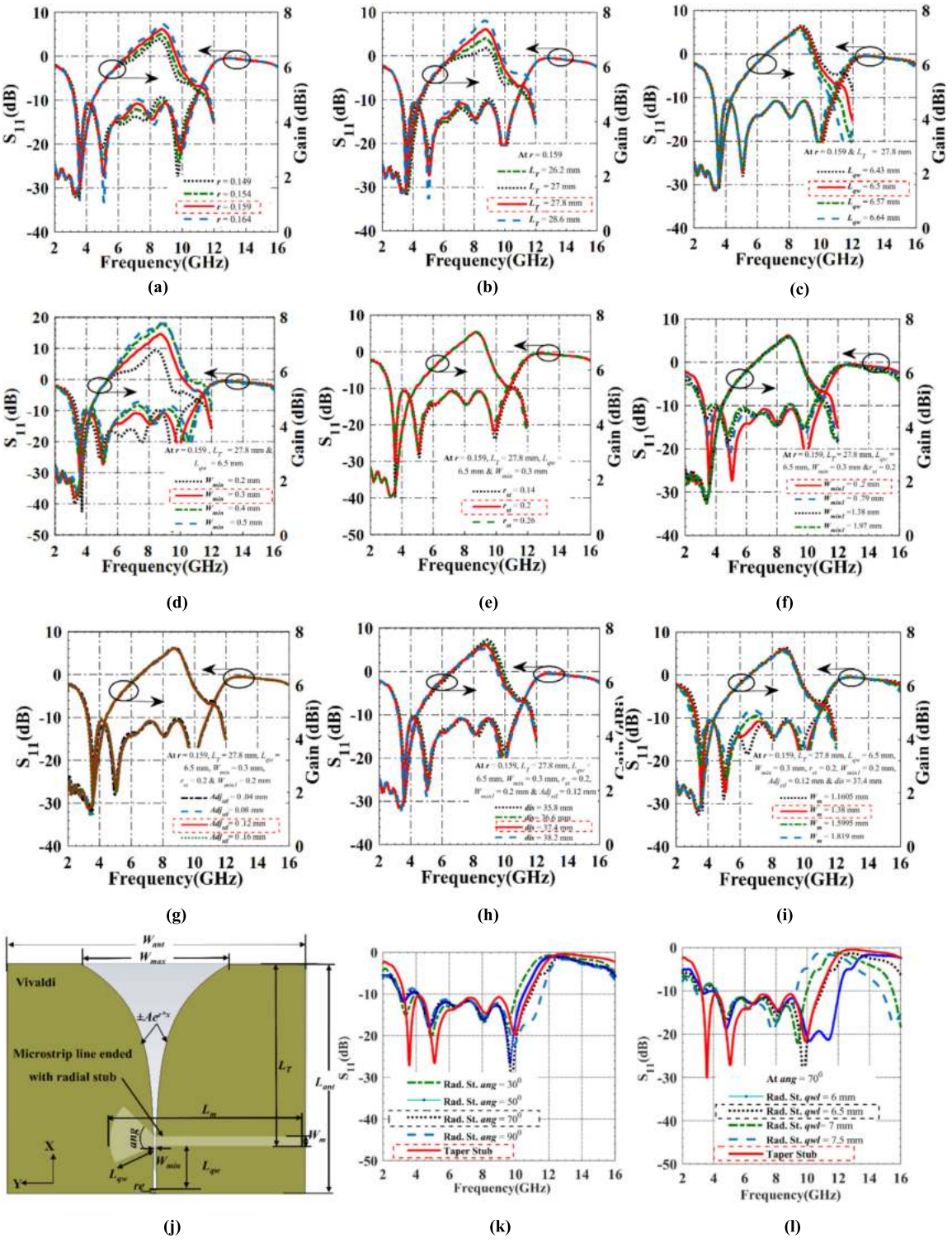

Fig. 5 Parametric study of the proposed UWB VTSA (Model B) in terms of S_{11} and gain on (a) r, (b) L_T, (c) L_{qw}, (d) W_{min}, (e) r_{st}, (f) W_{min1}, (g) Adj_{tsl}, (h) dis, and (i) W_m. Layout (j) and S_{11} parametric study on (k) ang and (l) L_{qw} of the UWB VTSA with (Radial/Tapered) M/S transition.

to one obtained at Adj_{tsl} = 0.12 mm. In this model, if only the stub is tapered and the slot is rectangular (which nearly at 0.04 mm), the matching is not good in addition to a slight shift in the band toward *Fh*. As illustrated in Fig. 5(h), the result for changing *dis* is the same as that for Model A where *dis* = 37.4 mm gives better matching. Fig. 5(i) shows that the best matching is obtained when W_m = 1.38 mm within the UWB frequency band. Although the BW is enhanced as W_m increases, $S_{11} > -10$ dB at the middle of the band. It can be observed that there is also a small increase in the gain when W_m decreases as at W_m = 1.1605 mm, however, W_m = 1.38 mm is selected due to its better S_{11}. λ/4 tapered

stub is replaced by the radial one in the transition of Model B as shown in Fig. 5(j). Fig. 5(k) shows the effect of changing *ang* where the best-obtained result is at *ang* = 70°. As illustrated in Fig. 5 (l), at *ang* = 70°, L_{qw} is changed and as it decreases or increases, the BW increases or decreases, respectively with a mismatch within UWB especially at 4 GHz. Also, there is a mismatch at the optimized value (L_{qw} = 6.5 mm). So, using the radial stub here also is not enhancing the performance of Model B. As a conclusion from the optimized parameters for Model B, the change of the transition shape helps only in reducing the total area (43.9 × 34.9 mm^2 = 1532.11 mm^2) by 1.51% from Model A by reducing L_{qw} from 6.52 mm (Model A) to 6.5 mm (Model B) and L_T from 28.6 mm (Model A) to 27.8 mm (Model B). This leads us to use other flexible shapes that have many parameters to be controlled such as in Model C and D.

3.3. UWB VTSA with (Trapezoidal/Rectangular) M/S Transition: (Model C)

The slot line shape here is selected to be rectangular due to its better performance as compared to the trapezoidal one and this will be explained later in the parametric studies in Fig. 6. Fig. 1(c) shows the layout of Model C. To transform the $\lambda/4$ rectangular stub to trapezoidal, two additional lengths are added to its widths, Adj_{trst1} (adjust the trapezoidal stub) and Adj_{trst2} and two additional lengths are added to the rectangular slot, Adj_{trsl1} (adjust the trapezoidal slot) and Adj_{trsl2} as shown in the inset of Fig. 1(c).

The best matching with enhanced BW is obtained at r = 0.161 (S_{11} < −10.434 dB, BW = (3.0911.284) = 8.194 GHz and maximum gain = 6.89 dBi), as shown in Fig. 6(a) despit of higher gain at r = 0.166 (7.1 dBi) than at r = 0.161 (6.89 dBi). Since using trapezoidal stub makes r different from that in Model A and B, it helps in changing and reducing the value of L_T as shown in Fig. 6(b) to be 26.4 mm for better matching although of higher gains at L_T = 27 mm (S_{11} < −10.275 dB BW = (3.1–11.3) = 8.2 G Hz and maximum gain = 7.15 dBi) and at L_T = 27.6 mm (S_{11} < −9.77 dB, BW = (3.11–11.31) = 8.08 GHz and maximum gain = 7.4 dBi). Fig. 6(c) shows that although the BW and the gain are 0.63% and 0.58%, respectively enhanced at L_{qw} = 6.45 mm (S_{11} < −10.375 dB, BW = (3.14–11.386) = 8.246 GHz and maximum gain = 6.93 dBi), L_{qw} = 6.51 mm (S_{11} < −10.434 dB, BW = (3.09–11.284) = 8.194 GHz and maximum gain = 6.89dBi) is selected due to its better matching. In terms of matching and gain there is no big difference between L_{qw} = 6.51 mm and the calculated one, L_{qw} = 6.57 mm (S_{11} < −10.48 dB, BW = (3.11–11.188) = 8.08 GHz and maximum gain = 6.88 dBi), however, L_{qw} = 6.51 mm is selected due its wider BW and smaller *Fl*. Finally, although the matching at L_{qw} = 6.63 mm (S_{11} < −10.625 dB, BW = (3.11–11.114) = 8 GHz and maximum gain = 6.88 dBi) is better, L_{qw} = 6.51 mm is selected due to its wider BW. W_{min} as shown in Fig. 6(d) has the same results obtained for Model B. Fig. 6(e) illustrates that at small values of Adj_{trst1}, S_{11} > −10 dB and the best S_{11} is obtained at Adj_{trst1} = 2.5 mm (S_{11} < −9.86 dB) with no big effect on the BW as Adj_{trst1} changes. Matching is enhanced when Adj_{trst2} is added as shown in Fig. 6(f) with a small increase in BW and gain as Adj_{trst2} increases. Adj_{trst2} = 1.5 mm (S_{11} < −10.434 dB, BW = (3.09–11.284) = 8.194 GHz and maximum gain = 6.89 dB) is selected which is better than at Adj_{trst2} = 1 mm (S_{11} < −10.382 dB, BW = (3.08–11.153) = 8.073 GHz and maximum gain = 6.89dBi) in terms of matching and BW. Although the matching and BW at Adj_{trst2} = 2 mm (S_{11} < −10.508 d B, BW = (3.125–11.396) = 8.271 GHz and maximum gain = 6.92dBi) and Adj_{trst2} = 2.5 mm (S_{11} < −10.45 dB, BW = (3.137–11.491) = 8.354 GHz and maximum gain = 6.91dBi) are better, Adj_{trst2} = 1.5 mm is selected due to its smaller *Fl*. Fig. 6(g) and (h), show that the rectangular slot (at Adj_{trsl1} = 0 mm and Adj_{trsl2} = 0 mm) is better than the trapezoidal slot. A direct comparison between using the rectangular (Adj_{trsl1} = 0 mm and Adj_{trsl2} = 0 mm) and trapezoidal (Adj_{trsl1} = 0.15 mm and Adj_{trsl2} = 0.3 mm) slots in terms of S_{11} and gain is shown in Fig. 6(k), where S_{11} in the rectangular slot is better than in trapezoidal one (mismatch at 4 GHz) and there is no big difference between their results in terms of gain. Fig. 6(i) shows that the best matching and a moderate gain (6.89 dBi) is obtained at *dis* = 36.85 mm although of the higher gain at *dis* = 35.15 mm (7.11 dBi) and *dis* = 36 mm (6.99 dBi). As illustrated in Fig. 6(j), W_m = 1.55 mm is selected due to the best obtained S_{11} although of the BW and gain enhancement at W_m > 1.55 mm.

Fig. 7(a) shows the microstrip feed line of Model C is ended by a $\lambda/4$ radial stub instead of the trapezoidal one. Best matching is achieved at *ang* = 30°, however, the BW is not enhanced (3–10 GHz) as shown in Fig. 7 (b). Fig. 7(c) indicates that through the UWB frequency band at all L_{qw} values, S_{11} is worse than that at trapezoidal stub. So no need to use the radial stub. Using the (Trapezoidal/Rectangular) M/S transition in Model C helps in reducing the antenna size and enhancing the BW (Area = 1442.15 mm^2 and BW = 7.65 GHz) by 7.3% and 6.64%, respectively from that in Model A (Area = 1555.64 mm^2 and BW = 7.65 GHz) and this due to the reduction in the antenna length and width parameters such as L_T from 28.6 mm (Model A) to 26.4 mm (Model C) and *dis* from 37.4 mm (Model A) to 36.85 mm (Model C). One can conclude that good selection of M/S transition shape in VTSA can enhance the antenna performance and reduce its size

3.4. UWB VTSA with (Circular/Circular) M/S Transition: (Model D)

As shown in Fig. 1(d), both microstrip stub and slot lines in M/S transition of this model have a circular shape with different radii, *radst* (radius of the circular stub), and *radsl* (radius of the circular slot), respectively. Only the stub has a $\lambda/4$ length where *radst* = 0.5 × L_{qw} . However, it is found that when *radsl* is < 0.5 × L_{qw}, the matching of the antenna is better which will be explained later in Fig. 8(e). The BW is enhanced when r increases as shown in Fig. 8 (a) and r = 0.17 (S_{11} < −10.84 dB, BW = (2.95–12.67) = 9.72 GHz and maximum gain = 6.63 dBi) is selected due its better maching although of enhanced gain at r = 0.18 (S_{11} < −10.135 dB, BW = (2.91–12.864) = 9.954 GHz and maximum gain = 7.11dBi). Due to the circular shape in the transition, r here is different from the other models and this helps in changing the other parameters such as L_T as shown in Fig. 8(b) where the best matching is obtained at L_T = 25 mm although of higher gains at L_T = 26 mm (S_{11} < −10.368 dB, BW = (2.95–12.74) = 9.

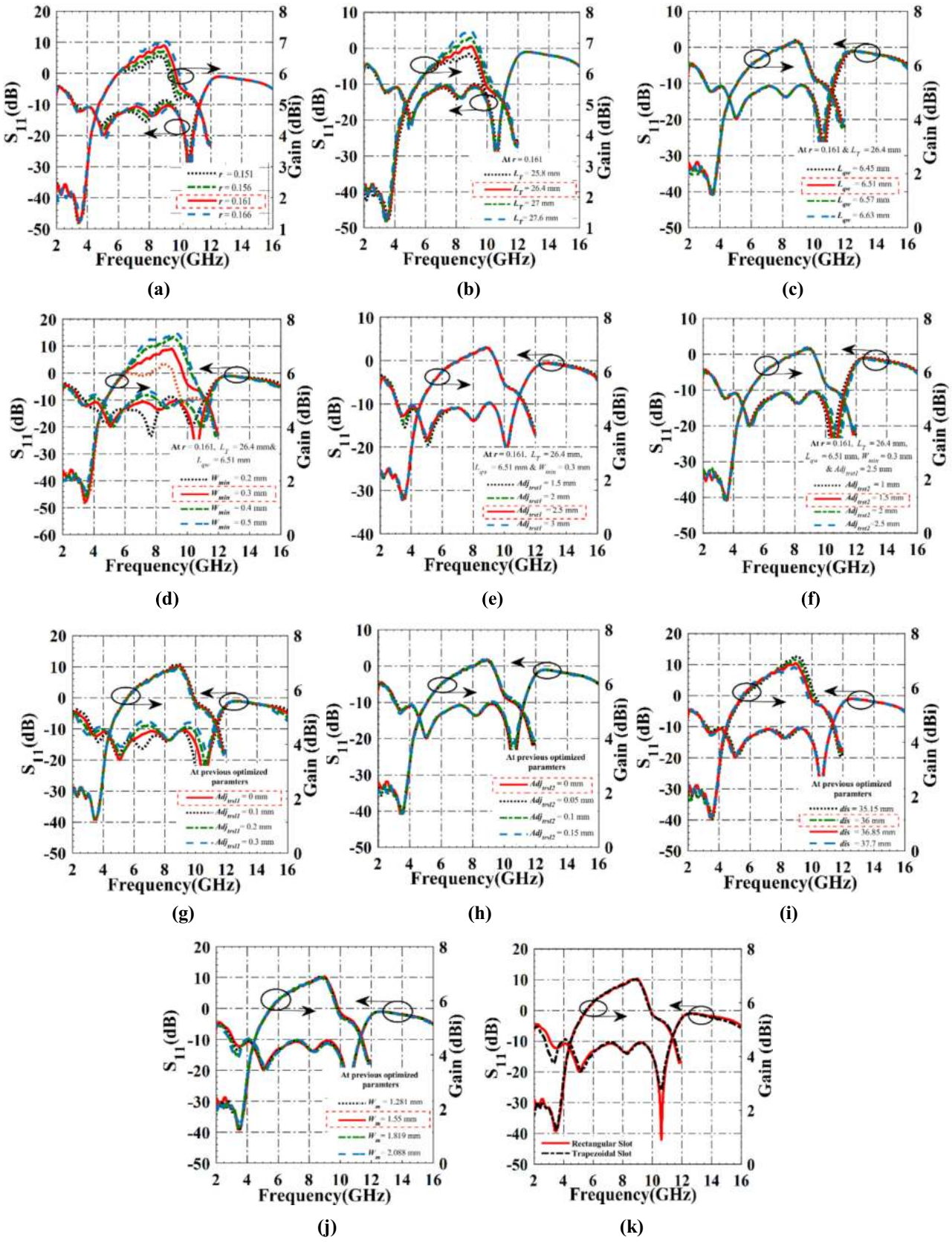

Fig. 6 Parametric study of the proposed UWB VTSA (Model C) in terms of S_{11} and gain on (a) r, (b) L_T, (c) L_{qw}, (d) W_{min}, (e) Adj_{trst1}, (f) Adj_{trst2}, (g) Adj_{trsl1}, (h) Adj_{trsl2} (i) dis, and (j) W_m. (k) Comparison between λ/4 rectangular and trapezoidal slot in the M/S transition in terms of S_{11} and gain.

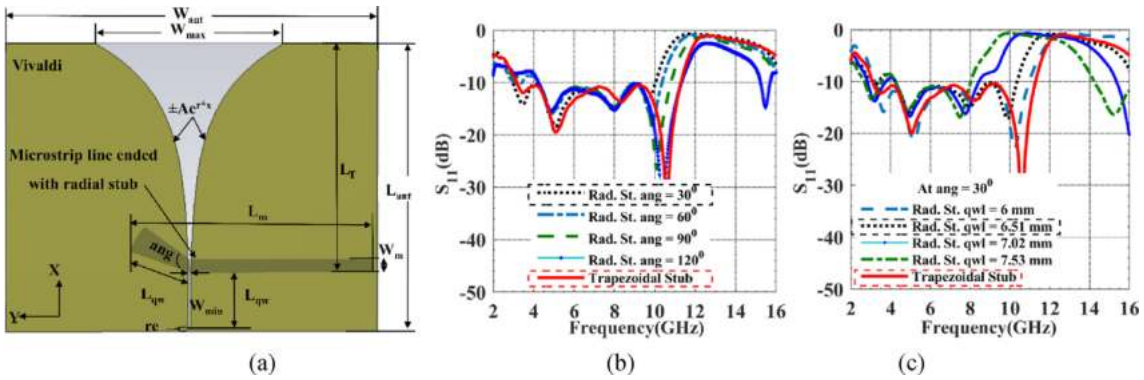

Fig. 7 Layout (a) and S_{11} parametric study on (b) *ang* and (c) L_{qw} of the UWB VTSA with (Radial/Trapezoidal) M/S transition.

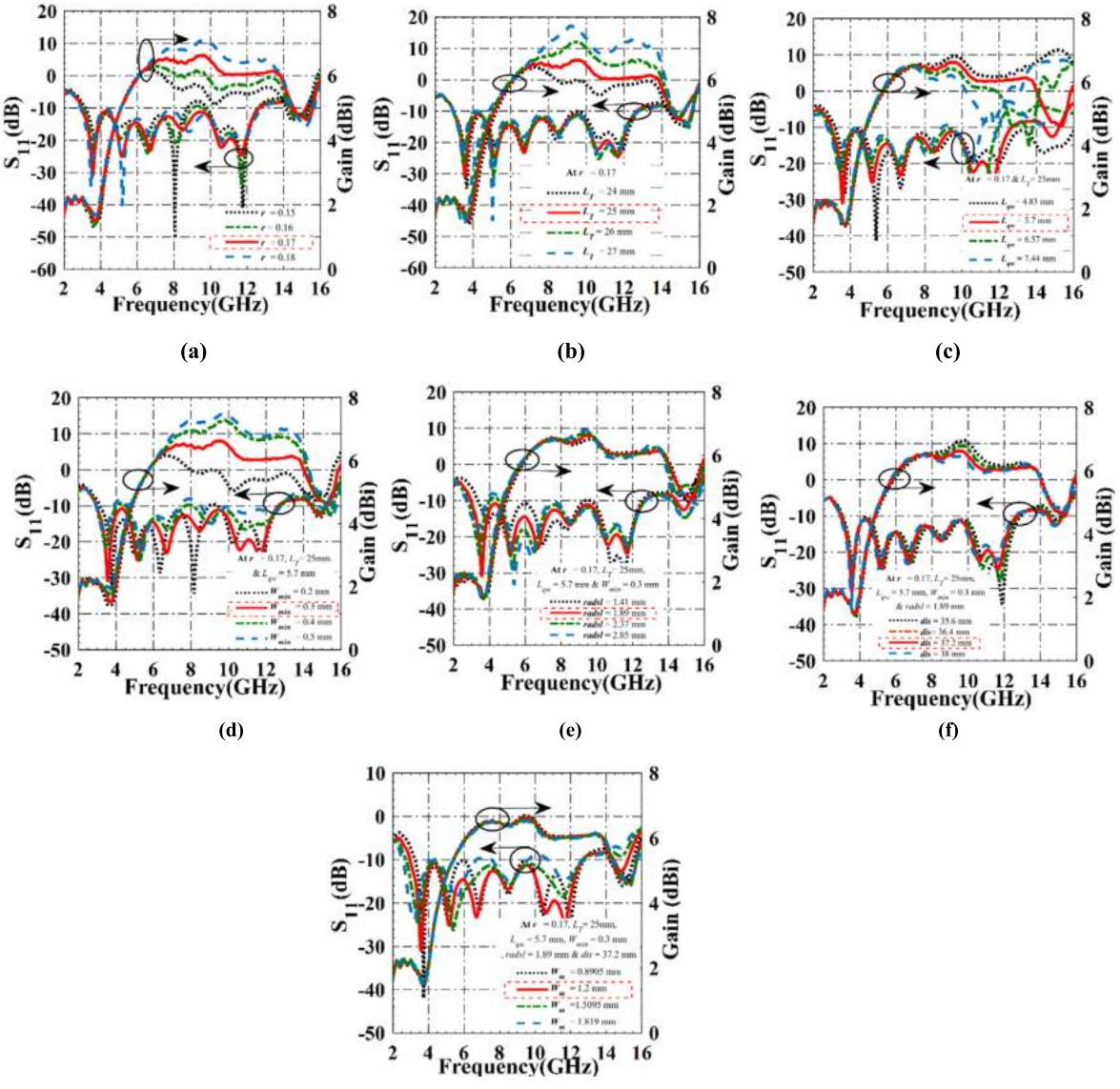

Fig. 8 Parametric study of the proposed UWB VTSA (Model D) in terms of S_{11} and gain on (a) *r*, (b) L_T, (c) L_{qw}, (d) W_{min}, (e) *radsl*, (f) *dis,* and (g) W_m.

79 GHz and maximum gain = 7.23 dBi) and L_T = 27 mm (S_{11} < −10.04 dB, BW = (2.93–12.765) = 9.835 GHz and maximum gain = 7.72 dBi). Fig. 8(c) shows that the best matching is obtained at L_{qw} = 5.7 mm (S_{11} < −10.84 dB, BW = (2.95–12.67) = 9.72 GHz and maximum gain = 6.63 dBi) despite of the enhanced gain and BW at L_{qw} = 4.83 mm (S_{11} < −10.33 dB, BW = (3.17–16.16) = 12.99 GHz and maximum gain = 6.82 dBi). As shown in Fig. 8(d), the best S_{11} within the UWB frequency band is obtained at W_{min} = 0.3 mm although of higher gains at W_{min} = 0.4 mm (S_{11} < −9.26 dB, BW = (2.94–12.74) = 9.66 GHz and maximum gain = 7.28 dBi) and W_{min} = 0.5 mm (S_{11} < −11 dB, BW = (3–12.66) = 9.66 GHz and maximum gain = 7.48 dBi).

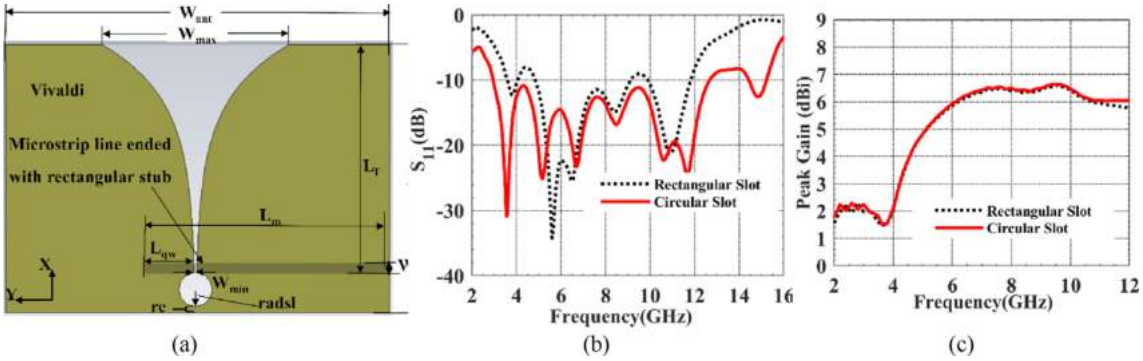

Fig. 9 Layout **(a)** and performance comparison of the UWB VTSA with (Rectangular/Circular) and (Circular/Circular) M/S transition M/S transition (b) S_{11} and (c) gain.

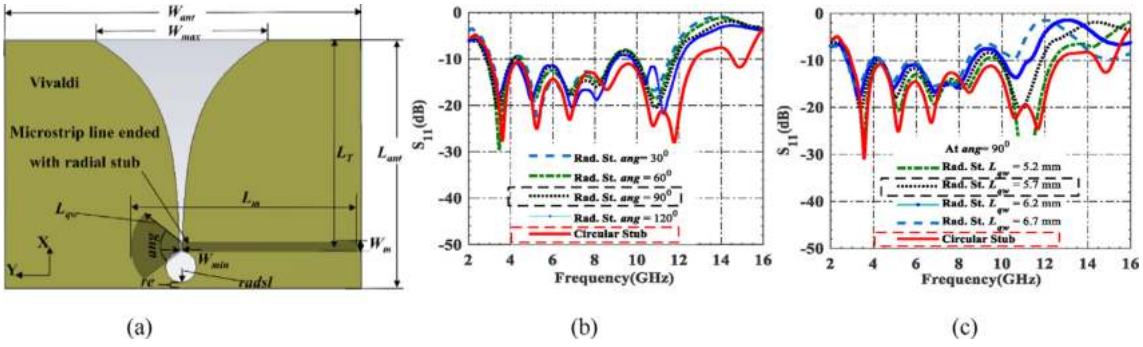

Fig. 10 Layout (a) and S_{11} parametric study on (b) *ang* and (c) L_{qw} of the compact UWB VTSA with (Radial/Circular) M/S transition.

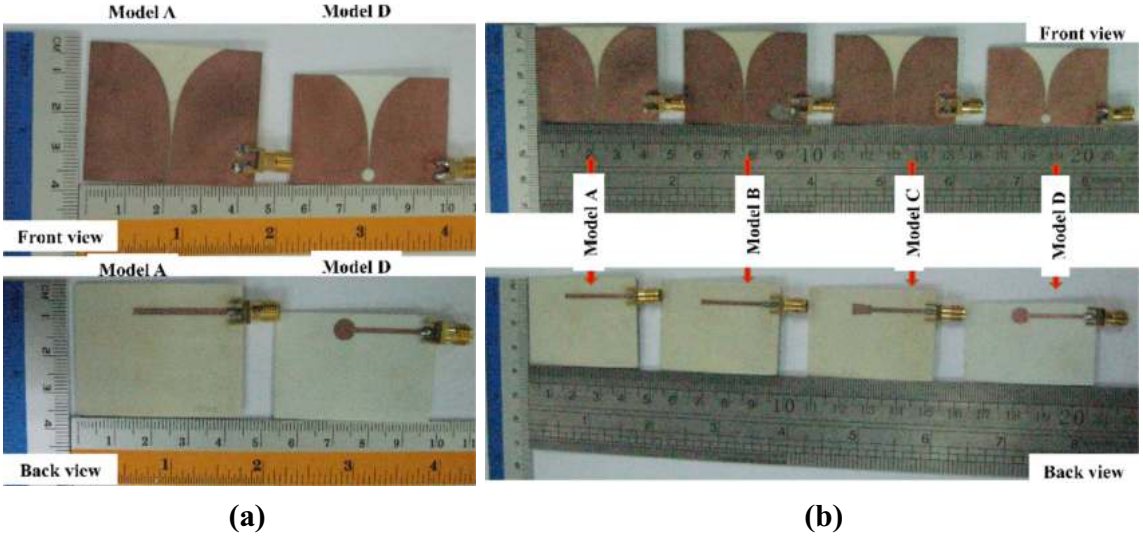

Fig. 11 Photograph of the fabricated UWB VTSA (a) Model D as compared to Model A, and (b) the four models (A-B).

Table 4 Comparison between the simulated and measured results for four models.

Antenna Models	S_{11}(dB) at Frequency Band (GHz)		Peak Realized gain (dBi)		Total efficiency (%)		Group Delay (ns) F2F	
	Meas.	Sim	Meas.	Sim	Meas.	Sim.	Meas.	Sim.
Model A, 1555.6464 mm^2	< −10 at 3.2–11, BW = 7.8	< −10.48, < 1.86 at 3.28–10.93, BW = 7.65	4.26–7.42	3.86–7.56	76.5–97	80–97	Around 1.25	Around 0.75
Model B, 1532.11 mm^2 (1.51%↓)	< −10 at 3.2–12.36, BW = 9.16 (14.85%↑)	< −10.66, < 1.83 at 3.23–10.83, BW = 7.61 (0.52%↓)	3.36–7.31 (1.5%↓)	3.75–7.39 (2.24%↓)	74.8–94	78.2–96	Around 1.25	Around 0.75
Model C, 1442.153 mm^2 (7.3%↓)	< −10.75 at 3.34–12.16, BW = 8.82(11.56%↑)	< −10.434, < 1.81 at 3.09–11.284, BW = 8.194 (6.64%↑)	2.86–6.66 (10.2%↓)	3–6.89 (8.86%↓)	82.9–92.96	80–96.24	Around 1.2	Around 0.75
Model D, 1256.112 mm^2 (19.25%↓)	< −11.58 at 3.14–13.48, BW = 10.7(24.56%↑)	< −10.84, < 1.8 at 2.95–12.71, BW = 9.72 (21.3%↑)	2.2–6.51 (12.26%↓)	2.1–6.63 (12.3%↓)	90.6–96.7	90.73–98	Around 1.1	Around 0.75

As in the previous models for best matching, both stub and slot length should be $\lambda/4$ (radii = 0.5 × L_{qw}), however, as shown in Fig. 8 (e), the best S_{11} is obtained at *radsl* = 1.89 mm (S_{11} < −10.84 dB , BW = (2.95–12.67) = 9.72 GHz and maximum gain = 6.63 dBi) which is better than at *radsl* = 1.41 mm (S_{11} < −9.86 dB , BW = (3.35–12.54) = 9.19 GHz and maximum gain = 6.56 dBi) in terms of matching, BW and gain and also better than at *radsl* = 2.37 mm (S_{11} < −9.2 dB , BW = (2.76–12.71) = 9.95 GHz and maximum gain = 6.75 dBi) and *radsl* = 2.85 mm (S_{11} < −8.1 d B , BW = (2.72–12.74) = 10.02 GHz and maximum gain = 6.8 dBi) in terms of matching. As illustrated in Fig. 8 (f), *dis* = 37.2 mm (S_{11} < −10.84 dB, BW = (2.95–12.67) = 9. 72 GHz and maximum gain = 6.63 dBi) is selected due its better matching as compared to that at *dis* = 35.6 mm (S_{11} < −10.3 dB, BW = (3.03–12.914) = 9.884 GHz and gain = 6.97 dBi) and *dis* = 36.4 mm (S_{11} < −10.54 dB, BW = (3–12.77) = 9.77 GHz and maximum gain = 6.8 dBi) despite their higher gain. Although at *dis* = 38 mm (S_{11} < −11.13 dB, BW = (2.92–12.55) = 9.63 GHz and maximum gain = 6.47 dBi) the matching is better, *dis* = 37.2 mm it is selected due to its better gain and to get more compactness. Fig. 8(g) illustrates that the best matching is obtained at W_m = 1.2 mm (S_{11} < −10.84 dB, BW = (2.95–12.67) = 9.72 GHz and maximum gain = 6.63 dBi) although of the higher gain at W_m = 0.8905 mm (S_{11} < −10.16 dB, BW = (3.23–12.74) = 9.51 GHz and maximum gain = 6.7 dBi).

Fig. 9(a) shows the antenna with (Rectangular/Circular) transition. As shown in Fig. 9(b) and 9 (c), the matching, BW and gain using circular stub (S_{11} < −10.84 dB, BW = (2.95–12.67) = 9.72 GHz and maximum gain = 6.63 dBi) are better than the rectangular one (S_{11} < −8.11 dB, BW = (3.6–11.82) = 8.22 GHz and maximum gain = 6.55 dBi). Using the radial stub and its effect on the antenna performance is shown in Fig. 10. Fig. 10(b) shows that at different values of *ang*, there is a mismatch. Since the best S_{11} is obtained at *ang* = 90, L_{qw} is changed and as shown in Fig. 10(c) at all L_{qw} there is a mismatch within the UWB frequency band. In conclusion, the radial stub may increase the BW if L_{qw} is decreased, however, the matching becomes worse.

The (Circular/Circular) M/S transition helps in reducing the antenna size (42.9 mm × 29.28 mm = 1256.112 mm^2) and enhancing the BW (9.72 GHz) by 19.25% and 21.3%, respectively as compared to Model A due to the reduction in the antenna length parameters (L_T = 25 mm and L_{qw} = 5.7-mm) which they are less than that in other models (Model A: L_T = 28.6 mm and L_{qw} = 6.52 mm, Model B: L_T = 27.8 mm and L_{qw} = 6.5 mm and Model C: L_T = 26.4 mm and L_{qw} = 6.51 mm). Based on the optimized parameters in Table 3, the four models are fabricated and tested and their prototypes are shown in Fig. 11(b). Fig. 11(a) shows the direct comparison between Model A and D. The final simulated and measured results of the four models will be discussed later by comparing them with the other models in Section 4

4. Results and discussion

Table 4 summarizes the simulated and measured results for the four models in terms of S_{11}, BW, peak realized gain, efficiency, and group delay. In addition, it displays the circuit area for each model and the obtained size reduction or BW enhance-

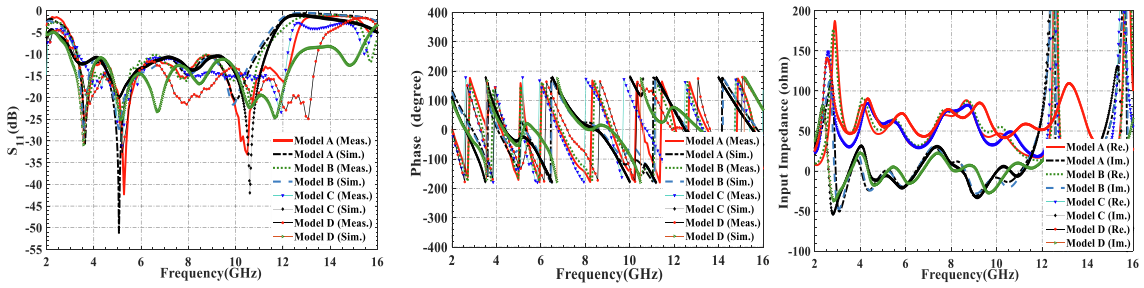

(a) (b) (c)

Fig. 12 Simulated and measured (a) S_{11}, (b) Phase, and (c) simulated input impedance of the proposed compact UWB VTSA four models.

ment percentages for Models B, C, and D as compared to Model A. It can be observed that as a penalty of reducing the size, the gain is a bit reduced, however, the antenna matching and BW are enhanced.

4.1. Reflection coefficient, input impedance, group delay and phase

All the four models provide good input matching of $S_{11} < -10$ dB as shown in Fig. 12. Although the gain is a bit reduced as a penalty of reducing the antenna sizes (from Model A to D), S_{11} and BW are enhanced (except for Model C where its measured BW is 3.7% less than that in Model B) and this is due to the use of different M/S transition shapes. The discrepancy between the simulated and measured results is due to fabrication tolerance and imperfect soldering of SMA connectors. As shown in Fig. 12(b), the four models have almost the same phase with a shift in Model D especially at high frequencies due to its smaller area as compared to the other models. The real and imaginary parts of the simulated input impedance shown in Fig. 12(c) are oscillating around 50 Ω and 0 Ω, respectively. This reflects that the different four microstrip feedlines with different ended stubs' shapes are matching properly with the 50 Ω SMA connecter (simulated as waveguide port in CST) which in turn leads to a good cou-

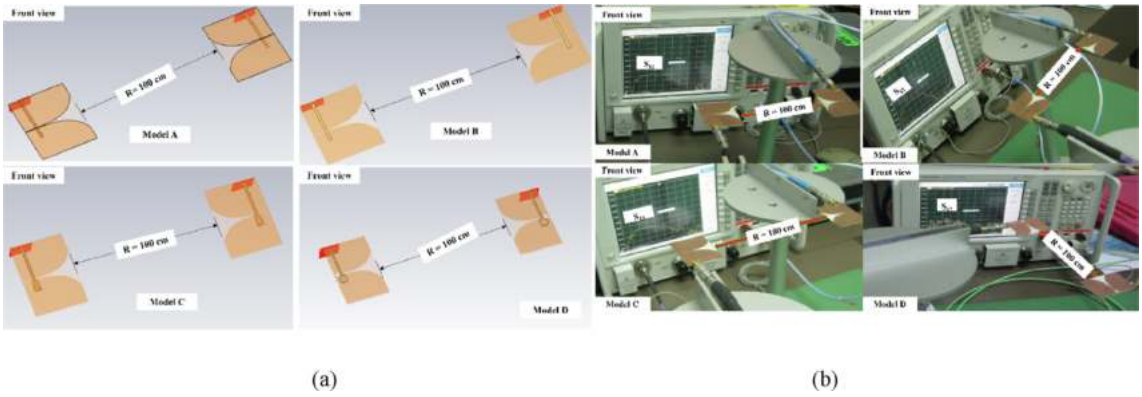

(a) (b)

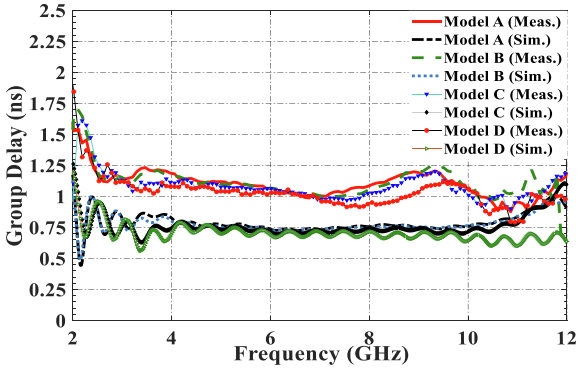

(c)

Fig. 13 (a) CST and (b) Measurement environments to calculate F 2 F group delay between the two samples of the four models (c) Simulated and measured group delay of the proposed four models.

pling of the signal to the slot resulting in the measured 7.8 GHz (Sim = 7.65 GHz), 9.16 GHz (Sim = 7.61 GHz), 8.82 GHz (Sim = 8.194 GHz) and 10.7 GHz (Sim = 9.72 GHz) wide impedance matching for Model A, Model B, Model C, and Model D, respectively.

In UWB application, group delay is an important factor where a nearly flat group delay within the UWB frequency band is required to guarantee the satisfactory of signal transmission [57]. To get the group delay for each model, 2 samples are designed, simulated, and fabricated. The two samples of each model are put in Face to Face (F 2 F) in the E- Plane, as shown in Fig. 13(a) and (b) in both simulation and measurement environment, respectively for all models. The distance (R) between the two models is taken in the far-field region and it is defined by[53]

$$R > \frac{2D^2}{\lambda} \tag{5}$$

where D is the largest dimension of the antenna and λ is the free space wavelength at f_c.

Fig. 13(c) shows approximate flat group delays where the measured ones are around 1.25 ns (Sim = 0.75 ns), 1.25 ns (Sim = 0.75 ns), 1.2 ns (Sim = 0.75 ns) and 1.1 ns (Sim = 0.75 ns) for Model A, Model B, Model C and Model D, respectively. As it is noticed that group delay is decreased from Model A to Model D and this due to the size reduction of the models which implies that the path that the signal takes to propagate becomes a little bit shorter. The measured group delay is greater than the simulated one in all models due to the fabrication and measurement tolerance in which the signal will face more losses during its propagation.

4.2. Gain, total efficiency, and radiation patterns

Fig. 14 shows the measurement setup in the anechoic chamber for Model A. The realized gain for all models is shown in Fig. 15(a), in which the gain is slightly reduced from Model A to D as a penality of the size reduction. It should be mentioned here that the gain is started at frequency f = 4 GHz because the waveguide probes at f < 4 GHz were not available during the measurement. The measured realized gain in Fig. 15 (a) for Model A, Model B, Model C and Model D, respectively started at f = 4 GHz from 4.26 dBi (Sim = 3.86 dBi), 3.36 dBi (Sim = 3.76 dBi), 2.86 dBi (Sim = 3. dBi) and 2.21 dBi (Sim = 2.17 dBi) then increased gradually due to the increase in the electrical dimensions [10] to reach its maximum value of 7.43 dBi (Sim = 7.56 dBi), 7.31 dBi (Sim = 7.38 dBi), 6.66 dBi (Sim = 6.89 dBi) and 6.51 dBi (Sim = 6.63 dBi) at f = 8.65 GHz, f = 8.65 GHz, f = 9 GHz and f = GHz 9.55, respectively and then it decreased due to the losses to 3.9 dBi (Sim = 4.2 dBi), 3.31 dBi (Sim = 3.76 dBi), 3.51 dBi (Sim = 3.8 dBi) and 5.81 dBi (Sim = 6 dBi) at f = 12 GHz. It can be observed that although a 19.25% size reduction is achieved for Model D, the gain is only reduced by 12.26%. So controlling the M/S transition shape from

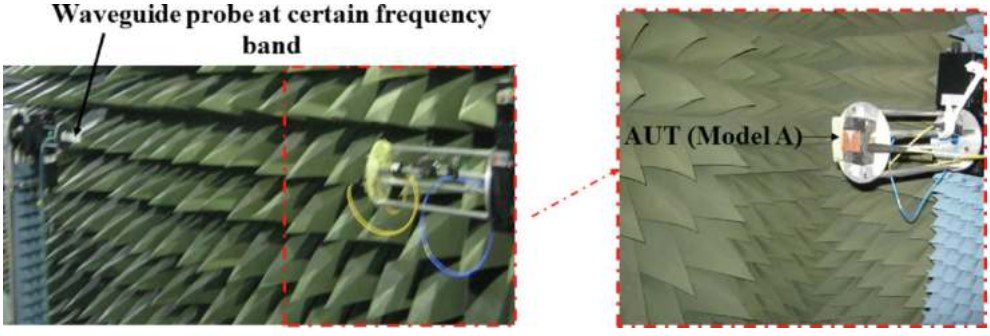

Fig. 14 Measurement environment for the AUT (Model A) at the anechoic chamber.

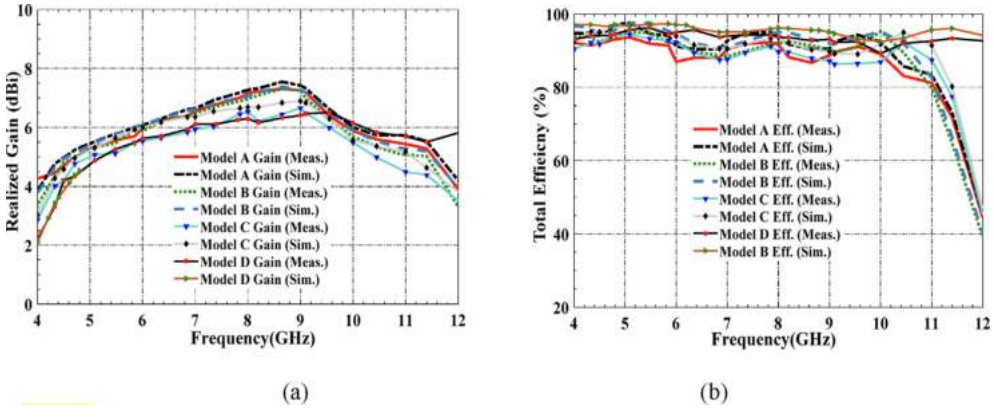

Fig. 15 Simulated and measured (a) realized gain and (b) total efficiency of the proposed compact UWB VTSA four models.

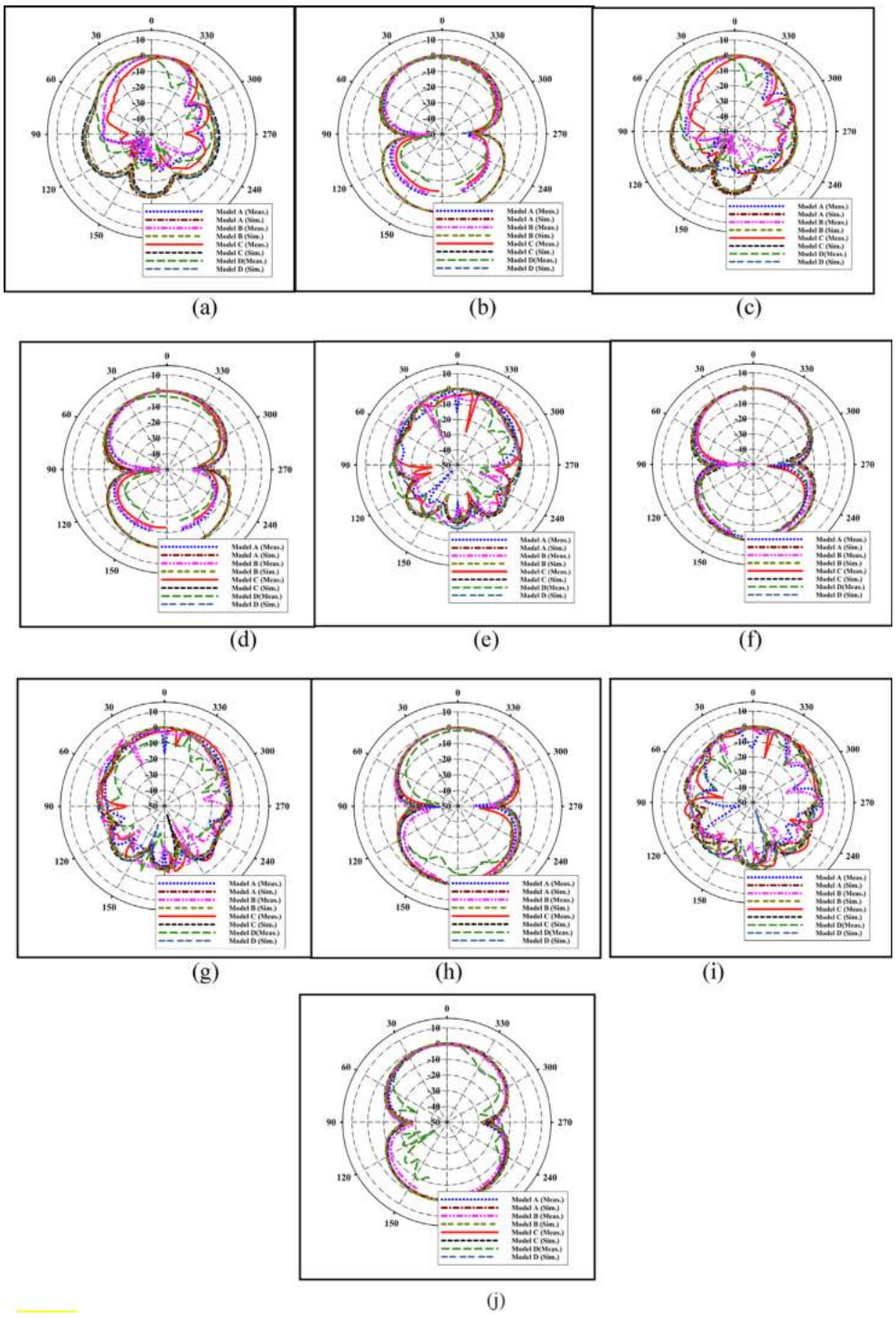

Fig. 16 Simulated and measured radiation pattern of the proposed compact UWB VTSA four models at $f = 5.11$ GHz (a) E and (b) H, $f = 5.48$ GHz (c) E and (d) H, $f = 8.2$ GHz (e) E and (f) H, $f = 8.8$ GHz (g) E and (h) H and $f = 10$ GHz (i) E and (j) H.

Model A to D helps in reducing the size of the antenna while keeping a moderate gain. Fig. 15(b) shows that the obtained measured total efficiencies for Model A, Model B, Model C, and Model D are between 76.5% and 97% (Sim: 80% and 97%), 74.8% and 94% (Sim: 78.2% and 96%), 82.9% and 92.96% (Sim: 80% and 96.24%) and 90.6% and 96.7% (Sim: 90.73% and 98%), respectively within the UWB frequency band.

It should be mentioned here that the cross-polarization is not considered in this work because NSI-MI anechoic chamber at Wireless Communication Centre (WCC), UTM-Johor Bahru that used for measuremnts doesn't consider the cross-

Table 5 Other related TSAs at different wide and ultrawide frequency bands in the literature.

Ref.	ε_r	S_{11}(dB)/VSWR at Frequency Band (GHz)	Gain(dBi)	Rad. Eff %	Method to enhance gain, matching, broaden BW	M/S transition	Size mm × mm × mm
This work	3.55	< −11.15 at 3–13.48	2.2–6.51	90.6–96.7	———	Circular/Circular	42.9 × 29.28 × 0.813
[58]	5.2	< −10 at 2.96–5.05/5.58–8.52	0–6.57	NA	semicircular patch embedment	Radial/Circular	40 × 45 × 0.8
[59]	4.4	< −10 at 2.5–11	4.4–8.4	NA	Corrugations	Radial/Circular	36 × 32 × 1.5
[45]	3.38	< −10 at 3.5–16.5	5.3–13.1	NA	Dielectric Sheets	Radial/Circular	34.5 × 28.4 × 1.524
[45]	3.38	< −10 at 3.5–16.5	5.72–15.3	NA	Dielectric Sheets with trapezoid-shaped profile	Radial/Circular	49 × 28.4 × 1.524
[40]	4.4	< −10 at 3.1–12	1.45–8.5	Sim.: 65–89	IA-ENZ-AM is added to the aperture	Radial/Circular	45 × 42 × 0.8
[12]	4.4	< −10.6 at 2.9–11	4.4–8.32	NA	Corrugations and grating elements	Radial/Circular	40 × 45x0.8
[25]	4.4	< −10 at 3–12.8	3.7–8.3	75–85	Two pairs of eye-shaped slots	Circular/Circular	36 × 36 × 0.8
[33]	4.4	VSWR < 2 at 2.5–10.6	5.1–8.2	60–82	———	Radial/Radial	41 × 48 × 0.8

*Rad. Eff. : Radiation efficiency and NA: Not Avialable.

polarization when they modeled the waveguide probes and according to that, the obtained measured cross-polarization was very bad and too big for all models. The normalized 2-D polar plots radiation patterns at E-plane (XY-plane) and H-plane (XZ-plane) are shown in Fig. 16(a) and (b), (c) and (d), (e) and (f), (g), and (h) and (i) and (j) at f = 5.11 GHz, 5.48 GHz, 8.2 GHz, 8.8 GHz, and 10 GHz, respectively for all four models. These frequencies are selected according to the available waveguide probes within the UWB frequency band during the measurement. As depicted in Fig. 16, stable end-fire and dipole shape radiation patterns are obtained in both E and H planes, respectively which guarantee the transmission and reception of the signal through the UWB frequency band. It can be also observed that due to higher order modes and losses at high frequencies (8.2 GHz, 8.8 GHz, and 10 GHz), SLLs are introduced to patterns especially in the E- plane and this is because the feed line works like a radiator and there will be a slight asymmetry at higher frequencies. The discrepancy between the simulated and measured radiation patterns is due to fabrication and measurement tolerance. These good features of the Model D in terms of compactness, good matching, moderate gain, and stable radiation patterns make it a good candidate for the modern wireless communication system that requires the antenna to be more reliable and compatible with the recent broadband applications such as UWB See Through Wall (STW), microwave and millimeter-wave imaging, and vehicular communication.

Finally, Table 5 illustrates the comparison of Model D with other recent works in the literature. The proposed antenna provides better S_{11}, higher realized gain, better radation efficiency wider BW, and smaller size than other works [12,25,33,40,58] except those who used techniques to enhance the gain and the BW which explains the higher gain in [45,59] although of their small area.

5. Conclusions

Simple Compact Ultra Wide Band (UWB) Vivaldi Tapered Slot Antenna (VTSA) using Circular/Circular Microstrip to Slot line (M/S) transition (Model D) is designed, analyzed, and fabricated in this paper. To analyze the effect of changing the transition's shape on the compactness and the performance of the proposed VTSA, it is designed using three other shapes (Model A: (Rectangular/Rectangular), Model B: (Taper/Taper), and Model C: (Trapezoidal/rectangular)) with detailed parametric studies. From Model A to D, the size is reduced with an enhanced matching and BW. As compared to Model A, the size of Model D is reduced by 19.25% and the obtained measured S_{11}(< −11.15 dB) and BW (10.48 GHz) are enhanced by 10.31% and 24.56%, respectively. Although the size is reduced, the obtained peak gain for Model D still moderate (6.51 dBi) and it is only reduced by 12.26% from that in Model A (7.42 dB). All the proposed four models provide good S_{11} < (between −10 and −11.15) dB with enhanced BW through the UWB frequency band. In addition, they provide stable end-fire radiation patterns and approximately flat group delays (1.1–1.25 ns). As future work, one may apply further miniaturization or gain enhancement techniques on Model D with its optimized parameters based on the study carried out in this paper.

Declaration of Competing Interest

The authors declare that they have no known competing financial interests or personal relationships that could have appeared to influence the work reported in this paper.

Acknowledgement

This work was supported by the Universiti Sains Malaysia through the RUI Grant numbers (1001/PELECT/8014058) and (304/PELECT/6315294).

References

[1] R. Kshetrimayum, An introduction to UWB communication systems, Ieee Potentials. 28 (2) (2009) 9–13.
[2] C. Jarufe, R. Rodriguez, V. Tapia, P. Astudillo, D. Monasterio, R. Molina, F.P. Mena, N. Reyes, L. Bronfman, Optimized corrugated tapered slot antenna for mm-wave applications, IEEE Trans. Antennas Propag. 66 (3) (2018) 1227–1235.
[3] S. Lin, S. Yang, A.E. Fathy, A. Elsherbini, Development of a novel UWB Vivaldi antenna array using SIW technology, Prog. Electromagn. Res. 90 (2009) 369–384.
[4] Y. Yang, Y. Wang, A.E. Fathy, Design of compact Vivaldi antenna arrays for UWB see through wall applications, Prog. Electromagn. Res. 82 (2008) 401–418.
[5] V. Mikhnev, Y. Maksimovitch, P. Vainikainen, A tapered-slot antenna with emulated continuous resistive loading, in: 2nd European Conf. Antennas Propag., IET, 2007: pp. 1–3.
[6] M. Serhir, Transient UWB antenna near-field and far-field assessment from time domain planar near-field characterization: Simulation and measurement investigations, IEEE Trans. Antennas Propag. 63 (11) (2015) 4868–4876.
[7] J. Shao, G. Fang, Y. Ji, K. Tan, H. Yin, A novel compact tapered-slot antenna for GPR applications, IEEE Antennas Wirel. Propag. Lett. 12 (2013) 972–975.
[8] X. Yin, X.Z. Su, W. Hong, T.J. Cui, An ultra wideband tapered slot antenna, in: 2005 IEEE Antennas Propag, Soc. Int. Symp., IEEE (2005) 516–519.
[9] J. Sun, W. Jiang, Design of a taper slotted low profile Vivaldi antenna for ultra-wideband near field imaging, in: 2013 Int, Conf. Commun, Conf. Commun. Circuits Syst., IEEE (2013) 428–430.
[10] M. Abbak, M.N. Akinci, M. Cayoren, I. Akduman, Experimental microwave imaging with a novel corrugated Vivaldi antenna, IEEE Trans. Antennas Propag. 65 (6) (2017) 3302–3307.
[11] M. Chiappe, G.L. Gragnani, Vivaldi antennas for microwave imaging: theoretical analysis and design considerations, IEEE Trans. Instrum. Meas. 55 (6) (2006) 1885–1891.
[12] G.K. Pandey, H.S. Singh, P.K. Bharti, A. Pandey, M.K. Meshram, High gain Vivaldi antenna for radar and microwave imaging applications, Int. J. Signal Process. Syst. 3 (2015) 35–39.
[13] H. Zhang, Microwave imaging for ultra-wideband antenna based cancer detection, 2015.
[14] H. Zhang, B. Flynn, A.T. Erdogan, T. Arslan, Microwave imaging for brain tumour detection using an UWB Vivaldi Antenna array, in: 2012 Loughbrgh, Antennas Propag. Conf., IEEE, 2012, pp. 1–4.
[15] P.A. Dzagbletey, J.-Y. Shim, J.-Y. Chung, Quarter-wave Balun Fed Vivaldi antenna pair for V2X communication measurement, IEEE Trans. Antennas Propag. 67 (3) (2019) 1957–1962.
[16] D.M. Elsheakh, E.A. Abdallah, Novel shape of Vivaldi antenna for water detection using GPR, in: 2nd Middle East Conf. Antennas Propag, IEEE, 2012, pp. 1–4.
[17] S.A. Çolak, N.T. Tokan, Time-domain analysis of modified vivaldi antennas, Antennas Wave Propag. (2018) 39–55.
[18] A.M. Abbosh, Miniaturized microstrip-fed tapered-slot antenna with ultrawideband performance, IEEE Antennas Wirel. Propag. Lett. 8 (2009) 690–692.
[19] J. Bai, S. Shi, D.W. Prather, Modified compact antipodal Vivaldi antenna for 4–50-GHz UWB application, IEEE Trans. Microw. Theory Tech. 59 (4) (2011) 1051–1057.
[20] A.M. De Oliveira, M.B. Perotoni, S.T. Kofuji, J.F. Justo, A palm tree antipodal Vivaldi antenna with exponential slot edge for improved radiation pattern, IEEE Antennas Wirel. Propag. Lett. 14 (2015) 1334–1337.
[21] E. Gazit. Improved design of the Vivaldi antenna, in: IEE Proc. H (Microwaves, Antennas Propagation), IET, 1988, pp. 89–92..
[22] J.D.S. Langley, P.S. Hall, P. Newham, Balanced antipodal Vivaldi antenna for wide bandwidth phased arrays, IEE Proc.-Microwaves, Antennas Propag. 143 (1996) 97–102.
[23] M. Moosazadeh, S. Kharkovsky, A compact high-gain and front-to-back ratio elliptically tapered antipodal Vivaldi antenna with trapezoid-shaped dielectric lens, IEEE Antennas Wirel. Propag. Lett. 15 (2016) 552–555.
[24] Y. Zhang, E. Li, C. Wang, G. Guo, Radiation enhanced Vivaldi antenna with double-antipodal structure, IEEE Antennas Wirel. Propag. Lett. 16 (2017) 561–564.
[25] K. Ma, Z. Zhao, J. Wu, M.S. Ellis, Z.P. Nie, A printed Vivaldi antenna with improved radiation patterns by using two pairs of eye-shaped slots for UWB applications, Prog. Electromagn. Res. 148 (2014) 63–71.
[26] C. Deng, Y. Xie, Design of resistive loading Vivaldi antenna, IEEE Antennas Wirel. Propag. Lett. 8 (2009) 240–243.
[27] Y.W. Wang, X.J. Gao, J.G. Liang, L. Zhu, Conformal corrugated edges for Vivaldi antenna to obtain improved low-frequency characteristics, Prog. Electromagn. Res. 60 (2015) 75–81.
[28] Y. Chareonsiri, W. Thaiwirot, P. Akkaraekthalin, Tapered slot antenna with squared cosine profile for ultra-wideband applications, in: 2014 11th Int, Conf. Electr. Eng. Comput. Telecommun. Inf. Technol., IEEE (2014) 1–4.
[29] Y. Chareonsiri, W. Thaiwirot, P. Akkaraekthalin, Design of ultra-wideband tapered slot antenna by using binomial transformer with corrugation, Frequenz. 71 (2017) 251–260.
[30] L. Pazin, Y. Leviatan, A compact 60-GHz tapered slot antenna printed on LCP substrate for WPAN applications, IEEE Antennas Wirel. Propag. Lett. 9 (2010) 272–275.
[31] F.C. Ren, F.S. Zhang, B. Chen, Q.C. Zhou, Compact tapered slot antenna for wideband applications, in: Proc. 2011 IEEE CIE Int. Conf. Radar, IEEE, 2011, pp. 1161–1163.
[32] J. Schorer, J. Bornemann, Broadband feed for low cross-polarization uniplanar tapered slot antennas on low-permittivity substrate, Wireless Engineering and Technology 4 (2013) 13–18.
[33] J. Wu, Z. Zhao, Z. Nie, Q.H. Liu, A printed UWB Vivaldi antenna using stepped connection structure between slotline and tapered patches, IEEE Antennas Wirel. Propag. Lett. 13 (2014) 698–701.
[34] A.S. Avdushin, A.V. Ashikhmin, V.V. Negrobov, Y.G. Pasternak, S.M. Fedorov, Vivaldi antenna with printed lens in aperture, Microw. Opt. Technol. Lett. 56 (2014) 369–371.
[35] S.H. He, W. Shan, C. Fan, Z.C. Mo, F.H. Yang, J.H. Chen, An improved Vivaldi antenna for vehicular wireless communication systems, IEEE Antennas Wirel. Propag. Lett. 13 (2014) 1505–1508.
[36] P. Gao, W. Dou, F. Wang, X. Chen, The miniaturization design of tapered slot antenna for wideband applications, in: 2015 Asia-Pacific Microw. Conf., IEEE, 2015, pp. 1–3.
[37] S. Ramesh, T.R. Rao, High gain dielectric loaded exponentially tapered slot antenna array based on substrate integrated waveguide for V-band wireless communications, AEU-Int. J. Electron. Commun. 69 (1) (2015) 48–55.

[38] B.R., Behera. Vivaldi antenna for UWB communications: Design, modelling and analysis of Vivaldi Antenna with genetic algorithm, in: 2016 Int. Conf. Control. Comput. Commun. Mater., IEEE, 2016, pp. 1–4.
[39] B. Zhou, H. Li, X. Zou, T.J. Cui, Broadband and high-gain planar Vivaldi antennas based on inhomogeneous anisotropic zero-index metamaterials, Prog. Electromagn. Res. 120 (2011) 235–247.
[40] G.K. Pandey, H.S. Singh, M.K. Meshram, Meander-line-based inhomogeneous anisotropic artificial material for gain enhancement of UWB Vivaldi antenna, Appl. Phys. A 122 (134) (2016) 1–9.
[41] X. Guo, T. Gao, Y. Yuan, Z. Xu, Analysis of Vivaldi antenna on cross-polarization application, in: 2016 11th Int, Symp. Antennas, Propag. EM Theory, IEEE (2016) 311–314.
[42] S. Ramesh, T.R. Rao, Dielectric loaded exponentially tapered slot antenna for wireless communications at 60 GHz, Prog. Electromagn. Res. 38 (2013) 43–54.
[43] M.A. Belen, İ.Ö. Evranos, F. Güneş, P. Mahouti, An UWB Vivaldi antenna with the enhanced functionalities through the use of DGS and dielectric lens, in: 2017 8th Int. Conf. Recent Adv. Sp. Technol., IEEE, 2017, pp. 199–201.
[44] P. Zhang, J. Li, Compact UWB and low-RCS Vivaldi antenna using ultrathin microwave-absorbing materials, IEEE Antennas Wirel. Propag. Lett. 16 (2017) 1965–1968.
[45] X. Li, D.W. Pang, H.L. Wang, Y. Zhang, G. Lv, Dielectric sheets covered broadband vivaldi antenna for gain enhancement, Prog. Electromagn. Res. 77 (2017) 69–80.
[46] R.P. Yadav, V. Kumar, R. Dhawan, Design and development of patch compensated wideband Vivaldi antenna, Int. J. Microw. Wirel. Technol. 10 (9) (2018) 1081–1087.
[47] X. Kang, Z. Li, An original Vivaldi antenna for 1–8GHz wideband application, in: 2015 IEEE 6th Int. Symp. Microwave, Antenna, Propagation, EMC Technol, IEEE, 2015, pp. 231–233.
[48] S. Nikolaou, G.E. Ponchak, J. Papapolymerou, M.M. Tentzeris, Conformal double exponentially tapered slot antenna (DETSA) on LCP for UWB applications, IEEE Trans. Antennas Propag. 54 (6) (2006) 1663–1669.
[49] A. Lazaro, R. Villarino, D. Girbau, Design of tapered slot Vivaldi antenna for UWB breast cancer detection, Microw. Opt. Technol. Lett. 53 (3) (2011) 639–643.
[50] G. Anur, S.S. Kumar, Tapered slotted Vivaldi antenna design using Fourier series approach for UWB applications, in: 2014 First Int, Conf. Comput. Syst. Commun., IEEE (2014) 7–11.
[51] Y.W. Wang, G.M. Wang, B.F. Zong, Directivity improvement of Vivaldi antenna using double-slot structure, IEEE Antennas Wireless Propag. Lett. 12 (2013) 1380–1383.
[52] P.J. Gibson, The vivaldi aerial, in: 1979 9th Eur. Microw. Conf., IEEE, 1979, pp. 101–105.
[53] C.A. Balanis, Antenna Theory: Analysis and Design, John wiley & sons, 2016.
[54] Y. Yang, Z. Zhao, X. Ding, Z. Nie, Q.H. Liu, Compact UWB slot antenna utilizing traveling-wave mode based on slotline transitions, IEEE Trans. Antennas Propag. 67 (1) (2019) 140–150.
[55] J. Shin, D.H. Schaubert, A parameter study of stripline-fed Vivaldi notch-antenna arrays, IEEE Trans. Antennas Propag. 47 (1999) 879–886.
[56] J.-S.G. Hong, M.J. Lancaster, Microstrip filters for RF/microwave applications, John Wiley & Sons, 2011.
[57] D.M. Elsheakh, N.A. Eltresy, E.A. Fattah, Ultra wide bandwidth high gain Vivaldi antenna for wireless communications, Prog. Electromagn. Res. 69 (2017) 105–111.
[58] J. Seo, J.H. Kim, J. Oh, Semicircular patch-embedded vivaldi antenna for miniaturized UWB radar sensors, Sens ors. 20 (2020) 5988.
[59] D. Yang, S. Liu, D. Geng, A miniaturized ultra-wideband Vivaldi antenna with low cross polarization, IEEE Access 5 (2017) 23352–23357.